Molecular Physics, 2013
Vol. 111, Nos. 14–15, 2163–2174, http://dx.doi.org/10.1080/00268976.2013.793889

INVITED ARTICLE

High resolution spectroscopy and perturbation analysis of the CO $A^1\Pi - X^1\Sigma^+$ (0,0) and (1,0) bands

M.L. Niu[a], E.J. Salumbides[a,b], D. Zhao[a], N. de Oliveira[c], D. Joyeux[c], L. Nahon[c], R.W. Field[d] and W. Ubachs[a,*]

[a]*Department of Physics and Astronomy, and LaserLaB, VU University, De Boelelaan 1081, 1081 HV Amsterdam, The Netherlands;* [b]*Department of Physics, University of San Carlos, Cebu City 6000, Philippines;* [c]*Synchrotron Soleil, Orme des Merisiers, St. Aubin BP 48, 91192, GIF sur Yvette cedex, France;* [d]*Department of Chemistry, Massachusetts Institute of Technology, Cambridge, MA 02139, USA*

(*Received 29 January 2013; final version received 3 April 2013*)

The two lowest-v' (0,0) and (1,0) bands of the $A^1\Pi - X^1\Sigma^+$ system of $^{12}C^{16}O$ have been investigated by two high-resolution spectroscopic methods. A vacuum ultraviolet Fourier-transform spectrometer, illuminated by synchrotron radiation, was applied to record a jet-cooled spectrum and a room temperature static gas spectrum, resulting in absolute accuracies of $0.01-0.02$ cm^{-1}. In addition two-photon Doppler-free laser spectroscopy has been applied to a limited number of rotational lines, resulting in an accuracy of 0.002 cm^{-1}. The data were used to perform an improved analysis of the perturbations in the $A^1\Pi$, $v = 0$ and $v = 1$ levels by vibrational levels in the $D^1\Delta$, $I^1\Sigma^-$, $e^3\Sigma^-$, $d^3\Delta$. and $a'^3\Sigma^+$ states.

Keywords: ultraviolet spectra; FT-spectroscopy; Doppler-free laser spectroscopy; perturbation analysis; carbon monoxide

1. Introduction

The $A^1\Pi - X^1\Sigma^+$ band absorption system of carbon monoxide has been known since its first observation as band heads in 1888 by Deslandres, who labelled it as the fourth positive system [1]. Simmons *et al.* recorded and analysed rotationally resolved spectra of the $A^1\Pi - X^1\Sigma^+$ (v', 0) bands in absorption up to $v' = 23$ [2]. The $A^1\Pi$ state was also investigated via the Ångstrom bands ($B^1\Sigma^+ - A^1\Pi$ system), initially by Birge [3], later by Kepa and Rytel [4], and thereafter with very high accuracy by Fourier-transform (FT) spectroscopy by Le Floch and Amiot [5]. In addition, information is extracted from the Herzberg bands ($C^1\Sigma^+ - A^1\Pi$ system) [6] and the $E^1\Pi - A^1\Pi$ system [7].

A comprehensive study of the perturbations in the $A^1\Pi$ state was performed by Field *et al.* [8], based on the knowledge available in 1972. For analysing the perturbations in the $A^1\Pi$ state the spectroscopic investigations of the perturbing states, observed in forbidden systems, are of relevance. Herzberg and Hugo observed the $a'^3\Sigma^+ - X^1\Sigma^+$ and $e^3\Sigma^- - X^1\Sigma^+$ systems [9], while Herzberg *et al.* observed the $d^3\Delta - X^1\Sigma^+$ system [10], Simmons and Tilford the $D^1\Delta - X^1\Sigma^+$ system [11] and Herzberg *et al.* the $I^1\Sigma^- - X^1\Sigma^+$ system [12].

Spectroscopic absorption and emission data of improved resolution were obtained by Le Floch and coworkers for some $A^1\Pi - X^1\Sigma^+$ bands, as well as the perturbing intercombination bands, at an absolute accuracy of 0.06 cm^{-1}. In particular, a very detailed perturbation analysis of the $A^1\Pi$, $v = 0$ state was performed for rotational states up to $J = 75$ [13] and for the specific rotation-electronic interaction between the $A^1\Pi$ and $D^1\Delta$ states [14]. Details of an analysis of the $A^1\Pi$, $v = 1$ state, as performed by Le Floch [15], can be found in the compilation of classical data by Morton and Noreau [16]. Notwithstanding the high accuracy of the data obtained from the classical studies, Drabbels *et al.* found small deviations for level energies of four (e)-parity levels of $A^1\Pi$, $v = 0$, $J = 1 - 4$ from a laser excitation study [17] performed at an accuracy of 0.002 cm^{-1}; values for these levels were found to deviate by -0.037 cm^{-1} from the classical data [13].

For targeted studies using the $A^1\Pi - X^1\Sigma^+$ bands of carbon monoxide to probe possible variations of the proton-to-electron mass ratio $\mu = m_p/m_e$ on cosmological time scales, an absolute accuracy of 0.01 cm^{-1} is required [18]. Therefore our team set out to remeasure the $A^1\Pi - X^1\Sigma^+$ spectra at high resolution and accuracy, and part of the data have been published recently in the context of searching for μ-variation [19]. Here we report a more extensive data set for the $A^1\Pi - X^1\Sigma^+$ (0,0) and (1,0) bands, as obtained from (i) a vacuum ultraviolet (VUV) FT study in both molecular jet and static gas configurations and (ii) a Doppler-free two-photon laser excitation study. By including highly accurate spectroscopic information on the $X^1\Sigma^+$ ground state of $^{12}C^{16}O$ obtained from infrared [20] and far-infrared studies [21] an improved analysis of the perturbations in the $A^1\Pi$, $v = 0$ and $v = 1$ states is presented.

---

[*] Corresponding author. Email: w.m.g.ubachs@vu.nl

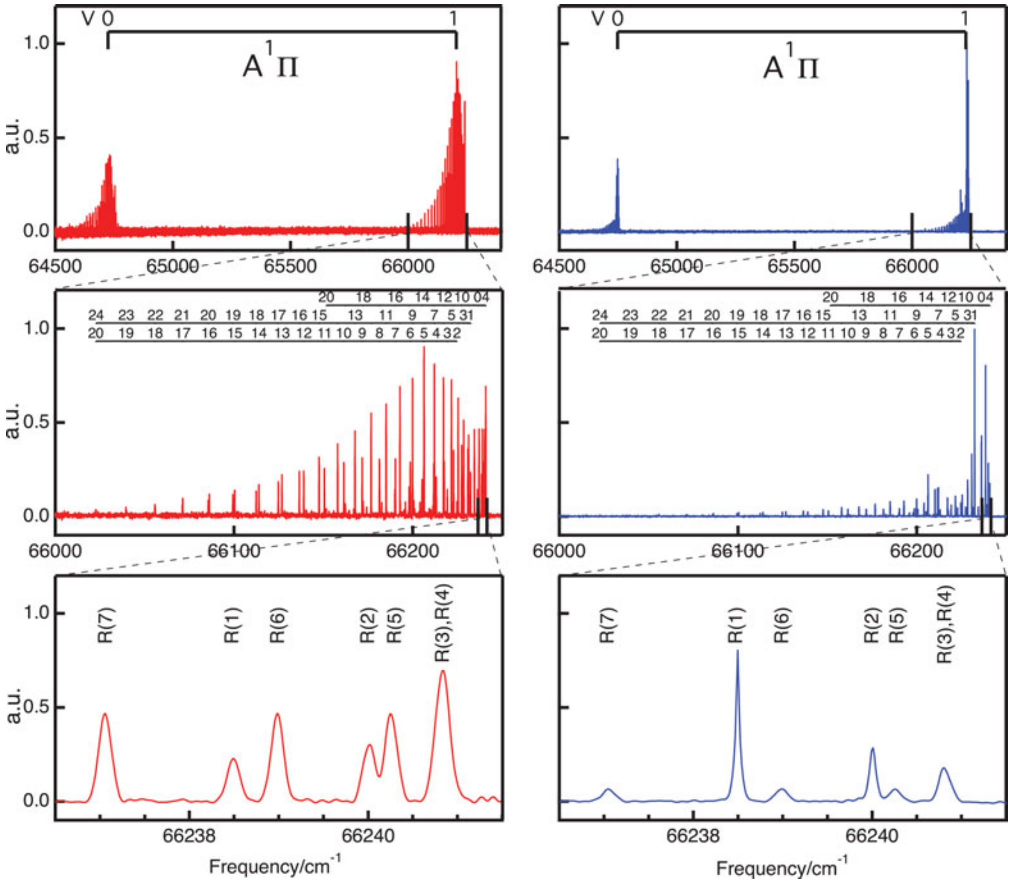

Figure 1. Spectra recorded with the vacuum ultraviolet Fourier-transform setup at the SOLEIL synchrotron. On the left the room temperature static gas absorption spectra are displayed, and on the right the jet absorption spectra. In the top row are overview spectra, in the middle panels a zoom-in on the (1,0) band, and the lower panels are detailed views of the spectra that demonstrate the linewidths. Note the narrow linewidth for the lowest *J*-levels in the jet spectra, and the increased linewidth for the higher *J*-levels, due to contributing absorption by background static gas.

2. Experimental

Two independent high-resolution spectroscopic studies of the $A^1\Pi - X^1\Sigma^+$ (0,0) and (1,0) bands were performed. The experimental methods have been described in Ref. [19], and are only introduced briefly here.

2.1. VUV-FT spectroscopy

The VUV-FT spectrometer installed at the of the SOLEIL DESIRS (Dichroïsme Et Spectroscopie par Interaction avec le Rayonnement Synchrotron) beamline synchrotron was used for recording direct absorption spectra, hence the transitions probed follow one-photon selection rules. For a detailed description of this instrument we refer to Refs. [22,23]. Of importance are the conditions and configurations under which the gas-phase absorption was monitored: a windowless cell-configuration and a free-jet configuration. A windowless T-shaped cell-configuration of 10 cm length was employed to record a spectrum from quasi-static CO gas. A free-jet configuration was used to measure the narrow lines characteristic of a jet-cooled beam, delivering spectra at a rotational temperature of 12 K, and with reduced Doppler width. Typical VUV-FTS spectra obtained from both configurations are shown in Figure 1.

In order to achieve optimum resolution in both configurations, each measurement was recorded by taking 1978 kilo-samples of data throughout the moving arm travel distance of ~40 mm. This setting produces an instrumental resolution of 0.075 cm^{-1} or resolving power of 900,000. When the travel distance of the moving arm is known [22,23], the wavelength of the FT spectrometer is intrinsically calibrated. Verification and further fine-tuning of the absolute calibration is obtained from on-line recording of a xenon line, which is produced in the gas filter employed for filtering the harmonics generated in the undulator section of the beam line. The calibration line is the Xe resonance at 68 045.156 (3) cm^{-1}[24], which is based on accurate relative measurements [25] and the measurement of a VUV anchor line [26].

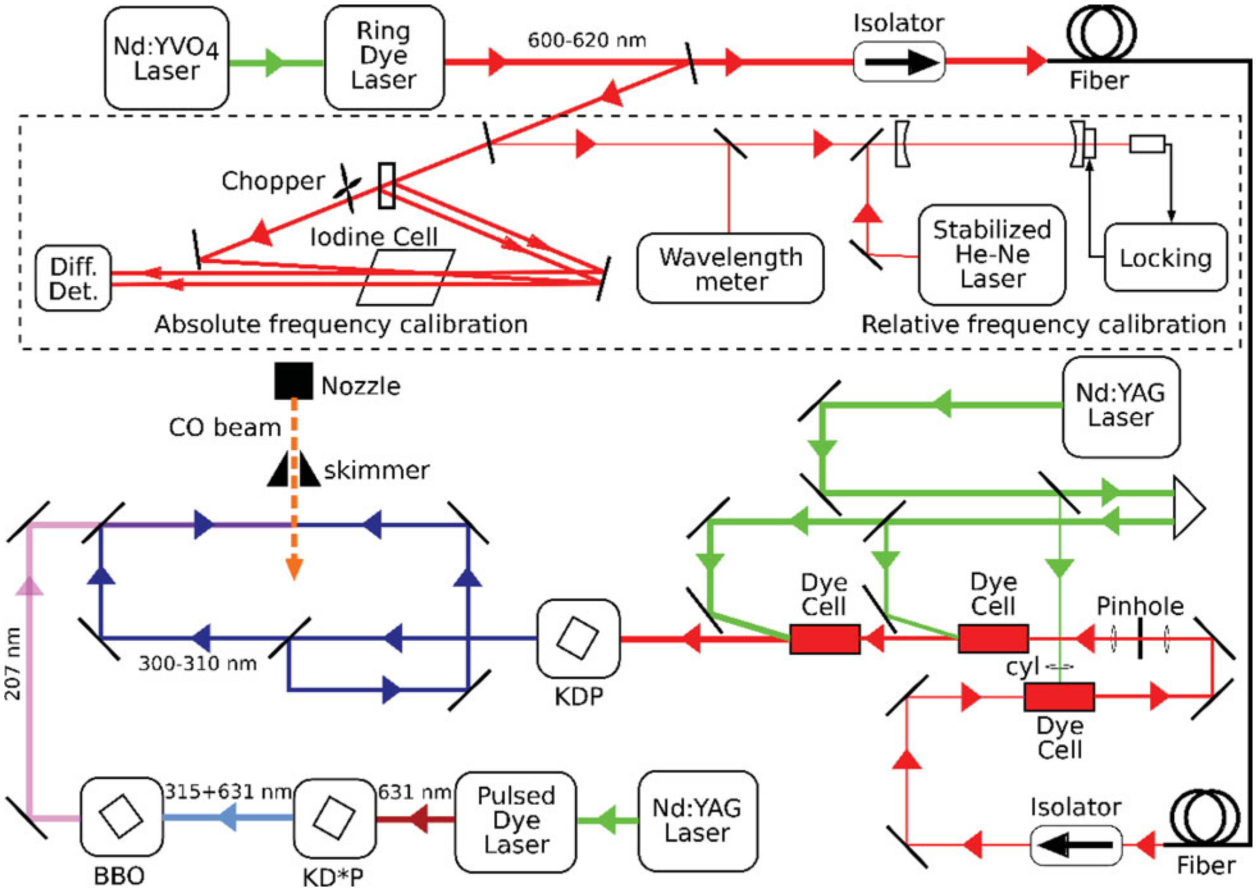

Figure 2. Experimental configuration employed for the 2+1' REMPI laser measurements. In the top part the CW ring dye laser, and the calibration facilities are shown. In the lower right part the pulsed dye amplifier (PDA) setup is depicted. The lower left part shows the interaction zone of the molecular beam with the two ultraviolet laser beams, and the Sagnac interferometric geometry for the frequency-doubled output of the injection-seeded PDA. The acronyms BBO, KDP and KD*P refer to crystals used for non-linear upconversion of laser radiation.

2.2. *Two-photon laser study*

Two-photon Doppler-free excitation studies on the CO $A^1\Pi - X^1\Sigma^+$ system were performed with the pulsed-dye-amplifier (PDA) laser system at Amsterdam, which has been used in several studies and described in previous publications (e.g. Ref. [27]). It consists of a three-stage narrowband tunable PDA, seeded by the output of a cw ring dye laser (Spectra Physics 380 D), and pumped by a Nd:YAG laser, delivering nearly FT limited laser pulses of 5 ns duration. For absolute frequency calibration of the seed laser I_2 saturated absorption spectra were recorded for reference [28,29], while transmission peaks of a length-stabilised etalon (of free spectral range 148.96 MHz) was employed for interpolation and for linearisation of the scan. The pulsed output of the PDA system was frequency doubled in a KDP crystal, and the tunable UV pulses were employed in the two-photon experiment.

Two-photon laser excitation is performed after splitting the UV-laser beam in two parts, each one perpendicularly crossing a pulsed and skimmed molecular beam, arranged from opposite sides as illustrated in Figure 2. Exact counter-propagation is achieved by aligning the beams as part of a Sagnac interferometer [30] to avoid residual Doppler-shifts. Considering the compromise between the signal-to-noise ratio and AC-Stark effects, each FT limited UV-laser beam is loosely focused with a 1-m lens. Another deep UV beam of 207 nm, generated by frequency tripling the 621 nm output of a pulsed dye laser system (Spectra-Physics PDL3), is employed for ionising the $A^1\Pi$ excited state population in a 2+1' resonance enhanced multi-photon ionisation (REMPI) scheme. It is noted that one photon at 207 nm suffices to ionise a molecule excited into the $A^1\Pi$ state. In order to avoid AC-Stark effects from the ionisation laser, its pulse timing is delayed by 10 ns with respect to the excitation laser. CO^+-ions, produced upon REMPI, are accelerated in a time-of-flight tube towards a multichannel plate (MCP) detector.

Sources of uncertainty in the absolute frequency calibration in the laser experiment were investigated. The statistical uncertainty associated with remeasurement of the

Table 1. Calibrated one-photon transition frequencies (in vacuum cm^{-1}) in the $^{12}C^{16}O$ $A^1\Pi - X^1\Sigma^+$ (0,0) and (1,0) bands from the VUV-FTS study. Lines marked with *b* were blended, and with *w* were weak in the spectrum. The estimated uncertainty is 0.01 cm^{-1}(1σ) except for the weak or blended lines.

J	$R_e(J)$	$Q_f(J)$	$P_e(J)$	$R_e(J)$	$Q_f(J)$	$P_e(J)$
		(0,0)			(1,0)	
0	64747.97			66236.22		
1	64750.50^b	64744.13		66238.49	66232.38	
2	64752.35	64742.83^b	64736.44	66240.01	66230.80	66224.69
3	64753.54	64740.86	64731.25	66240.79^b	66228.48	66219.27
4	64754.01	64738.23	64725.44	66240.85^b	66225.41	66213.09
5	64753.73	64734.93	64718.92^b	66240.25	66221.64	66206.20^b
6	64752.62	64730.95	64711.72	66238.99	66217.19	66198.58
7	64750.33^b	64726.26	64703.77	66237.06	66212.08	66190.29^b
8	64745.87	64720.84	64694.96	66234.47	66206.30^b	66181.35^b
9	64752.11	64714.60	64684.97	66231.24	66199.89	66171.72
10	64747.30	64707.40	64672.84	66227.35	66192.81	66161.47
11	64742.66^b	64698.87	64671.40	66222.81	66185.09	66150.55
12	64737.56	64688.26	64658.92	66217.60	66176.71	66138.99
13	64731.83	64693.70	64646.61	66211.73	66167.67	66126.77
14	64725.02	64682.70	64633.88	66205.18	66157.96	66113.91
15	64716.31	64671.99	64620.44^w	66197.96	66147.59	66100.36
16	64717.69^w	64661.11	64606.02^w	66190.03^b	66136.54	66086.16
17	64708.31	64649.80		66181.47^b	66124.81	66071.28^b
18	64699.22	64638.02		66172.23	66112.41	66055.77^b
19		64625.66		66162.28	66099.33	66039.54^w
20		64612.68^w		66151.64^w	66085.57	66022.67^w
21		64599.05^w			66071.07^b	
22					66055.94^{wb}	
23					66039.81^w	

lines is found to be 0.001 cm^{-1}. The dominant source of systematic uncertainty is the effect of frequency chirp in the PDA [27], amounting to 0.002 cm^{-1} in the presently used two-photon excitation mode; this estimate is deduced from quantitative investigations of this phenomenon [31]. A second source is in the AC-Stark effect, which is studied in detail. Measurements of the transition frequency as a function of power density are shown for the example of the S(0) and R(2) lines in the $A^1\Pi - X^1\Sigma^+$ (0,0) band in Figure 3. The S(0) transition frequency plotted in Figure 3 is offset by 64,754 cm^{-1}, while that for R(2) is offset by 64,752 cm^{-1}. It is noted that in view of experimental limitations the power density can only be given on a relative scale in Figure 3. The AC-Stark measurements were used for extrapolation to zero power density, yielding the true transition frequencies. The fitting uncertainty of the extrapolated AC-Stark value is 0.0007 cm^{-1}. The possible Doppler-shift in a two-photon experiment on a molecular beam is minimised by employing the Sagnac interferometric scheme to ascertain that laser beams are counter-propagating [30]. The other sources of uncertainty such as line-fitting, I_2 calibration, etalon non-linearity and

Table 2. Transition frequencies (in vacuum cm^{-1}) in the $e^3\Sigma^- - X^1\Sigma^+$ (1,0) band of $^{12}C^{16}O$ obtained in the VUV-FT experiment.

J	$^QR_e(J)$	$^QQ_f(J)$	$^OP_e(J)$
		(1,0)	
8	64758.42	64755.88	
9			64701.24
10			64685.42
11		64718.75^b	
12		64705.73	
13		64674.65	

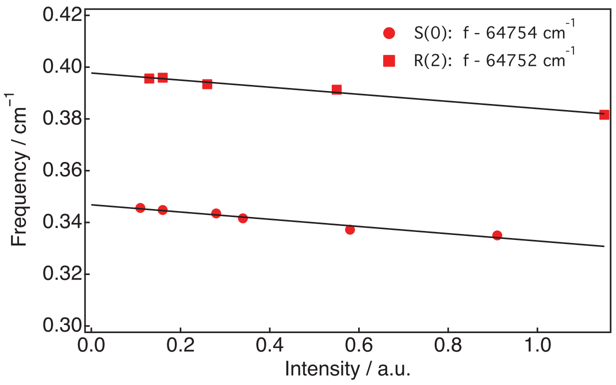

Figure 3. Assessment of the AC-Stark effect on the two-photon S(0) and R(2) lines in the $A^1\Pi - X^1\Sigma^+$ (0,0) band of CO. The true value of the transition frequency is determined from extrapolation to zero intensity.

Table 3. Transition frequencies (in vacuum cm^{-1}) in the $d^3\Delta - X^1\Sigma^+$ (5,0) band of $^{12}C^{16}O$ obtained in the VUV-FT experiment. In the $d^3\Delta - X^1\Sigma^+$ system only the F_3 components are observed, corresponding to transitions to the $^3\Delta_1$ spin-orbit component.

J	$R_e(J)$	$Q_f(J)$	$P_e(J)$
		(5,0) F_3	
0	66210.20^w		
2		66204.06	
3	66211.29	66200.58	
4	66209.16^w	66195.89	
5	66205.78^w		
6	66201.09^w	66182.70	66166.90^w
7		66174.17	66155.80^w
8		66164.35^w	66143.42^w
9		66153.06^w	
10		66140.53^w	

DC-Stark shift make very small contributions. The overall uncertainty in the strongest laser lines with good signal-to-noise ratio is estimated to be 0.002 cm^{-1}.

3. Results

3.1. VUV-FT data

VUV-FT spectra for the $A^1\Pi - X^1\Sigma^+$ (0,0) and (1,0) bands of CO are recorded in a molecular jet expansion and in a room temperature static gas cell. Overview spectra for both configurations are shown in Figure 1. It is noted that in the jet-cooled spectrum, the spectral contributions from background gas give rise to broadened pedestals to the narrow lines. From the Boltzmann distribution a rotational temperature of 320 ± 20 K and a linewidth of 0.16 cm^{-1} are deduced for the static cell configuration. For the jet-configuration a bi-modal temperature distribution is found, as a consequence of some room temperature background gas residing in the VUV beam path. The rotational temperature of the jet component is 12 ± 1 K, while for the room temperature pedestal a rotational temperature of 340 ± 60 K is derived. The linewidth of the jet part of the spectral lines is 0.09 cm^{-1}, while the pedestal exhibits a width of 0.16 cm^{-1}.

Some 118 transitions of CO $A^1\Pi - X^1\Sigma^+$ (0,0) and (1,0) bands, measured with the VUV-FTS, are presented in Table 1. In addition 23 absorption lines of excitations to perturber states are listed in Tables 2 and 3. The subscripts *e* and *f* in Tables 1–3 indicate the electronic symmetry of the upper state to emphasise that the FTS and two-photon laser transitions (see Table 5 and detailed descriptions below) obey different selection rules and thus access different upper states for a given lower state. The superscripts *Q* and *O* in Table 2 denote the $e^3\Sigma^-$ total angular momentum excluding spin, according to the notation in Ref. [16]. Accurate line positions in these tables are obtained by fitting the FTS data with a model that correctly describes the recorded convolved profiles. The accuracy of these transitions is 0.02 cm^{-1}. A few weak (denoted by *w*) and blended (*b*) lines have larger error of 0.04 cm^{-1}. As will be discussed below, the transition frequencies of low-*J* lines in the $A^1\Pi - X^1\Sigma^+$ bands are accurate at the 0.01 cm^{-1} level.

The data obtained by the FTS methods are analysed for internal consistency. Combination differences between

Table 4. Two-photon transition frequencies ν (in vacuum cm^{-1}) in the CO $A^1\Pi - X^1\Sigma^+$ (0,0) and (1,0) bands and in transitions to perturbing states as obtained from the Doppler-free laser measurements.

J	$S_e(J)$	$R_f(J)$	$Q_e(J)$	$P_f(J)$	J	$S_e(J)$	$R_f(J)$	$Q_e(J)$	$P_f(J)$
		$A^1\Pi - X^1\Sigma^+$(0,0)					$A^1\Pi - X^1\Sigma^+$(1,0)		
0	64754.347				0	66242.347			
1	64760.049	64750.518	64744.138		1	66247.707	66238.503	66232.383	
2		64752.398	64742.815	64736.450	2	66252.333	66240.017	66230.813	66224.694
3		64753.612	64740.825		3		66240.800	66228.481	
4		64754.156			4		66240.876	66225.419	
5		64754.017			5		66240.267		
6		64753.176			6		66238.994		
7		64751.591			7			66212.085	
8		64749.190			9		66231.249		
9		64745.822			13		66211.731		
10		64741.128			17	66241.303			
11		64734.360			19	66228.352			
12		64743.640					$d^3\Delta - X^1\Sigma^+$(5,0)		
13		64736.459			1		66211.750		
		$e^3\Sigma^- - X^1\Sigma^+$(1,0)			2		66212.117		
10		64761.036			3	66224.547	66211.268		
11		64751.832			4	66225.005			
					5	66224.151			

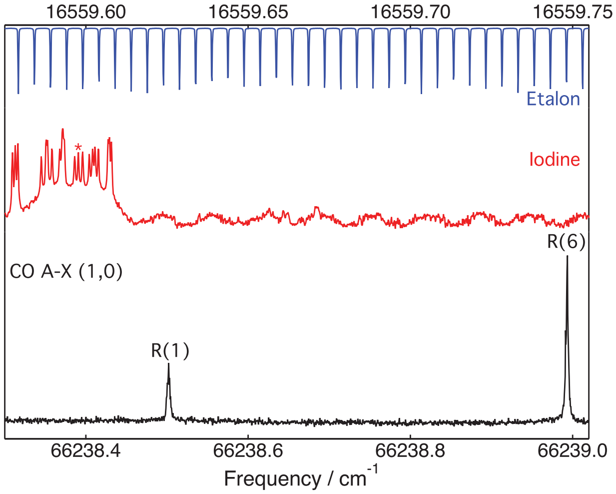

Figure 4. Two-photon excitation spectrum of close lying R(1) and R(6) lines in the $A^1\Pi - X^1\Sigma^+$ (1,0) band of $^{12}C^{16}O$ recorded simultaneously with an I_2 saturated absorption spectrum for absolute reference [28] and the transmission markers of a HeNe-stabilised etalon for relative calibration. The I_2 hyperfine component indicated with an asterisk (*) was used for absolute reference. The scale on top represents the frequency of the cw-seed laser, the one at the bottom the two-photon excitation energy.

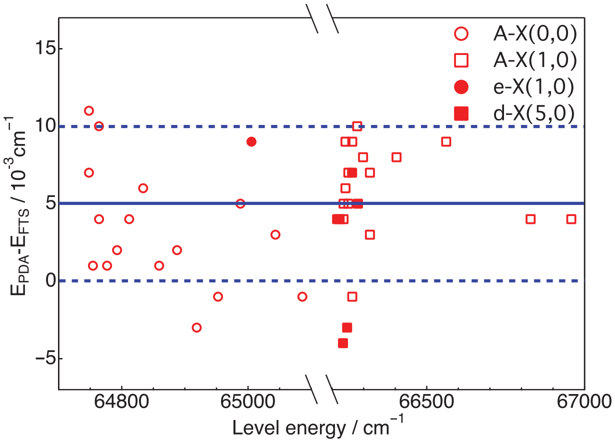

Figure 5. Comparison of level energies as obtained from the Doppler-free two-photon laser experiments (E_{PDA}) and those from the VUV-FT data (E_{FTS}).

P(J) and R($J - 2$) lines in the VUV-FT spectra, probing a common excited state $J' = J - 1$, were calculated and compared to the very accurate far-infrared data [21] yielding a standard deviation of 0.013 cm^{-1}. Apart from some outlier points, associated with very weak or blended lines, this analysis demonstrates that the relative accuracies of the low-J values in the FT-spectra are 0.01 cm^{-1}.

3.2. Two-photon laser data

In the two-photon Doppler-free excitation studies spectral lines in the CO $A^1\Pi - X^1\Sigma^+$ (0,0) and (1,0) bands were investigated. A typical example of a spectrum, covering the R(1) and R(6) lines in the $A^1\Pi - X^1\Sigma^+$ (0,0) band, is shown in Figure 4. Transition frequencies were obtained by producing a linearised absolute scale for the two-photon energy from the simultaneously recorded I_2 and etalon spectra at the fundamental frequency provided by the cw seed-laser, and then fitting the CO resonances on that scale, after multiplying by four. Results (including AC-Stark correction) at an accuracy of 0.002 cm^{-1} are presented in Table 4. In the laser experiments some transitions to $e^3\Sigma^-$ and $d^3\Delta$ perturbing states were also observed. It is noted that the frequencies in the VUV-FT one-photon spectra and the two-photon laser spectra are different, e.g. the R(1) line observed by both methods probes a different Λ-doublet component in the excited $^1\Pi$ state, and therefore exhibits a different

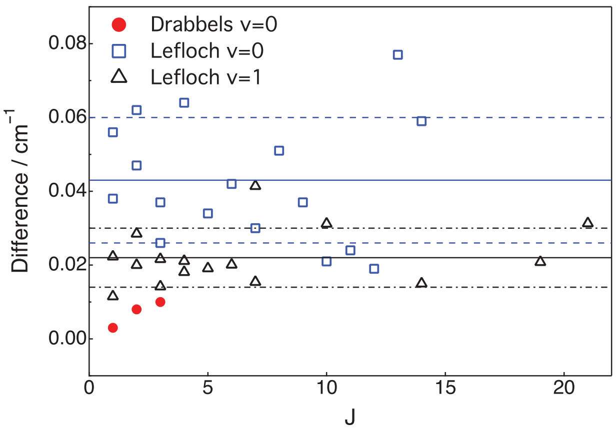

Figure 6. Comparison of level energies obtained in the present laser study with those of Le Floch [13,15] and Drabbels [17]. The solid line indicates the average deviation for each band, the dashed ($v = 0$) and dash-dotted ($v = 1$) lines indicate 1σ.

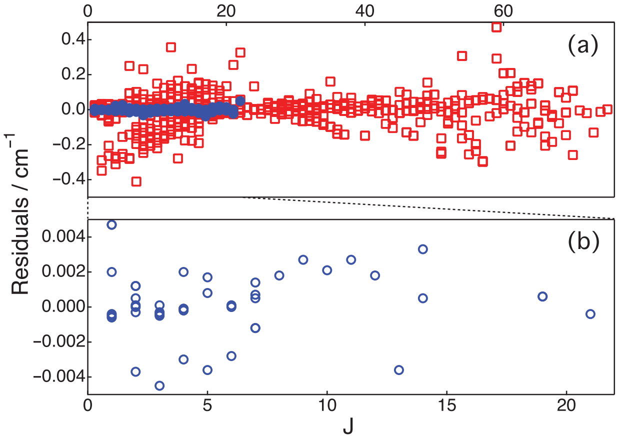

Figure 7. Fitting residuals from the current perturbation model used. Data points from the FTS and the laser study state are represented by circles in (a), data from literature are represented by open squares. The residuals for transitions of the present laser study only are shown on a reduced scale in (b).

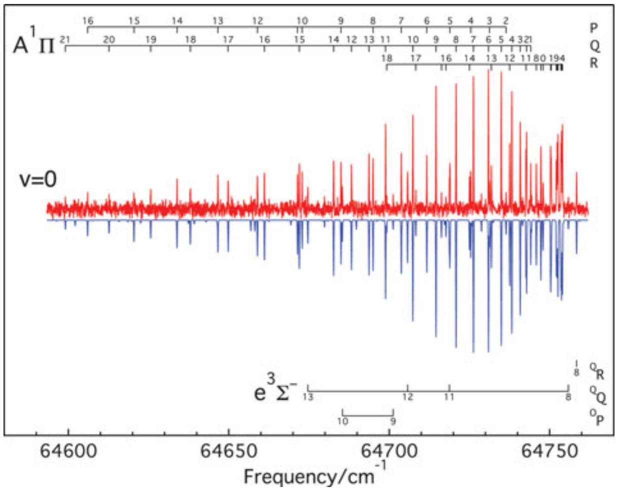

Figure 8. Simulated spectrum (lower trace) with FTS spectrum (upper) for $A^1\Pi - X^1\Sigma^+$ (0,0) band of CO.

transition frequency. Further, in two-photon excitation the R(0) transition is forbidden [32]. Ground state combination differences were also calculated and compared to accurate far-infrared data, resulting in a standard deviation of only 0.002 cm^{-1}and thus proving consistency within the laser data set.

3.3. *Level energies*

Using the accurately known level energies in the ground state [21], both the one-photon transition frequencies and the two-photon transition frequencies are converted to level energies, listed in Table 5, in order to make a detailed comparison of accuracies. The FTS data are benchmarked against the laser data in Figure 5. This demonstrates that there is an average offset between the two data sets of 0.005 cm^{-1}, which is attributed to an offset in the VUV-FT data, well within the estimated uncertainty. The deviations have a (1σ) spread of 0.01 cm^{-1}, showing that the VUV-FT data can be considered reliable within this uncertainty limit.

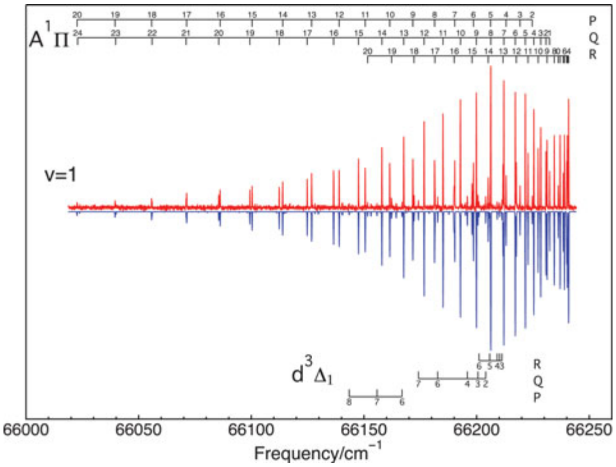

Figure 9. Simulated spectrum (lower trace) with FTS spectrum (upper) for $A^1\Pi - X^1\Sigma^+$ (1,0) band of CO.

In a comparison of the present $A^1\Pi$ $v = 0$ level energies from laser data with that of Ref. [13], we obtain an average difference of 0.043 cm^{-1} with a standard deviation 0.017 cm^{-1}. The latter value is consistent with the statistical uncertainty claimed in Ref. [13]. The discrepancy could be attributed to the accuracy of the absolute reference standard used in that study [33]. A similar comparison of the $A^1\Pi$ $v = 1$ level energies of the present laser data with those in Ref. [15] yield a difference of 0.022(8) cm^{-1}. The comparison of the level energies from Le Floch *et al.* [13,15] is shown graphically in Figure 6. The average discrepancy with the Le Floch data is different for the $v = 0$ and $v = 1$ bands, precluding the possibility of applying a global correction to all previous measurements of the other bands, e.g. those listed in Ref. [16]. In the following section, we discuss a deperturbation analysis which also included the high$-J$ $A^1\Pi$ level energies from [13,15], which were corrected for by taking into account the average discrepancy in the comparison for each band.

The present laser spectroscopic data can be compared to the results of the laser measurements performed by Drabbels *et al.* [17], probing the $B^1\Sigma^+ - A^1\Pi$ (0,0) band. The results of a previous investigation from the same group [34] of the $B^1\Sigma^+ - X^1\Sigma^+$ system are then used to derive the $A^1\Pi$ level energies. A comparison of the transitions derived for the $A^1\Pi - X^1\Sigma^+$ system from Ref. [17,34] and the present laser data set yields an average difference of 0.0035 cm^{-1} with a standard deviation of 0.013 cm^{-1}. We note that excluding the $B^1\Sigma^+ - A^1\Pi$ P(2) transition of table 1 in Ref. [17] reduces the standard deviation of the comparison to 0.0034 cm^{-1} and the average difference is -0.0017 cm^{-1}. The $A^1\Pi$ level energies listed in table 2 of Ref. [17] are slightly different than a derivation from the combination of the $B^1\Sigma^+ - X^1\Sigma^+$ (from Ref. [34]) and $B^1\Sigma^+ - A^1\Pi$ (from Ref. [17]) spectroscopic investigations. Using these listed $A^1\Pi$ level energies of Drabbels *et al.* [17], a comparison with the present laser data yield an average difference of 0.007(4) cm^{-1}(the datapoints are included in Figure 6). Although we do not find exact agreement with Drabbels *et al.* [17], nevertheless the overall shift in $A^1\Pi$, $v = 0$ levels with respect to those of Le Floch *et al.* [13] is confirmed.

4. Perturbation analysis

Previous studies [8,13,14,16,35] have shown that the $A^1\Pi$ state of CO is perturbed by $D^1\Delta$, $I^1\Sigma^-$, $e^3\Sigma^-$, $d^3\Delta$and $a'^3\Sigma^+$ states. In the analysis, we have adopted an effective Hamiltonian model with matrix elements given in Table 6. For the $A^1\Pi$ state the subscript i refers to vibrational quantum numbers $v = 0$ and 1, the e and f electronic symmetry components of the $A^1\Pi$ state are treated

Table 5. Level energies (in vacuum cm^{-1}) of $A^1\Pi$ and perturbing states calculated from the combined data sets form the two experiments. Levels indicated with (*) are derived from the more accurate Doppler-free two-photon laser excitation study. The other levels are derived from the VUV-FTS study. Where possible values are obtained after averaging over transitions frequencies in different branches. *e* and *f* denote the electronic symmetry of the state.

J'	e	f	e	f	F_{1e}	F_{2f}	F_{3e}	F_{3f}
	$A^1\Pi, v = 0$		$A^1\Pi, v = 1$		$e^3\Sigma^-, v = 1$		$d^3\Delta, v = 5$	
1	64747.983 *	64747.985 *	66236.228 *	66236.229 *			66210.20	
2	64754.349 *	64754.363 *	66242.348 *	66242.348 *				66215.595 *
3	64763.894 *	64763.933 *	66251.551 *	66251.552 *				66223.652 *
4	64776.60	64776.681 *	66263.868 *	66263.870 *			66234.36	66234.338 *
5	64792.46	64792.605 *	66279.32	66279.324 *			66247.617*	
6	64811.41	64811.687 *	66297.93	66297.937 *			66263.453*	66263.44
7	64833.35	64833.911 *	66319.728 *	66319.730 *			66281.822*	66281.81
8	64857.95	64859.233 *	66344.70	66344.69	64874.22	64894.27		66302.74
9	64884.26	64887.580 *	66372.87	66372.87	64896.82			66326.04
10	64925.08	64918.800 *	66404.21	66404.227 *				66351.93
11	64958.69	64952.532 *	66438.76	66438.76		64972.440 *		
12	64996.32	64988.027 *	66476.47	66476.47		65005.499 *		
13	65037.34	65043.406 *	66517.37	66517.36		65024.35		
14	65081.53	65086.157 *	66561.42	66561.429 *				
15	65128.48	65133.05	66608.64	66608.64				
16	65177.37	65183.59	66659.01	66659.01				
17	65240.16	65237.52	66712.53	66712.53				
18	65296.03	65294.81	66769.20	66769.20				
19	65356.01	65355.34	66829.024 *	66829.00				
20		65419.06	66891.96	66891.95				
21		65485.96	66958.030 *	66957.98				
22				67027.17				
23				67099.18				

separately, and the + and − signs pertaining to Lambda doubling in the diagonal element refer to the *e* and *f* symmetry states, respectively. While the $D^1\Delta$ and $d^3\Delta$ states have nearly degenerate *e* and *f* components, the $I^1\Sigma^-$ state exhibits only *f* components, two fine structure levels of the $e^3\Sigma^-$ state have *e* character and one has *f*, and for the $a'^3\Sigma^+$ state there are two *f* and one *e* levels. The interactions between the $A^1\Pi$ state and the $D^1\Delta$ and $I^1\Sigma^-$ states are due to L-uncoupling and thus produce heterogeneous interactions with *J*-dependent matrix elements, while interaction with the triplet states is due to spin-orbit interaction represented by *J*-independent matrix elements [8]. Note that the matrix is symmetric, the lower left non-diagonal elements (not shown) are equivalent to those of the corresponding upper right elements. An approximation is made by neglecting the mutual interactions between the perturbing states, therefore the corresponding matrix elements are set to zero.

In this study highly accurate level energies of $A^1\Pi$, low-*J* levels are determined (up to $J = 21$ for $v = 0$ and to $J = 23$ for $v = 1$, respectively), while in previous investigations the rotational manifold could be followed to much higher *J*-values. For $A^1\Pi$, $v = 0$ values up to $J = 75$ were listed [13], while for $A^1\Pi$, $v = 1$ extensive measurements were performed, and a listing of up to $J = 70$ is available in a Thesis study [15]. Representations in terms of molecular constants are given in the open literature [10,14,16,36].

In the perturbation analysis, a least-squares fitting procedure using the Pgopher software [37] was applied to the experimental data. It turned out to be necessary to include literature data from Le Floch and co-workers [13,15] to constrain fitting of the parameters pertaining particularly to the perturber states that cross the $A^1\Pi$ rotational manifolds at high-*J* values. Also included in the global fitting are level energies for the $J = 22$–75 states for the $A^1\Pi$ $v = 0$ state from Ref. [13] and level energies from $J = 24$–70 states for the $A^1\Pi$ $v = 1$ state from Ref. [15]. For the $A^1\Pi$ $v = 0$ state, the perturbing states as in the previous work of Le Floch *et al.* [13] are comprised in the fit, namely the $D^1\Delta$ $v = 0$ and 1, the $I^1\Sigma^-$ $v = 1$ and 2, the $e^3\Sigma^-$ $v = 1$, 2 and 3, the $d^3\Delta$ $v = 4$ and 5, and the $a'^3\Sigma^+$ $v = 9$ states. While for the $A^1\Pi$ $v = 1$ state, we also include the perturbing states as indicated in Figure 1 of Ref. [35], which are the $D^1\Delta$ $v = 1$ and 2, the $I^1\Sigma^-$ $v = 2$ and 3, the $e^3\Sigma^-$ $v = 3$, the $d^3\Delta$ $v = 5$ and 6 and the $a'^3\Sigma^+$ $v = 10$ and 11 states. We have also included transitions from the ground state $X^1\Sigma^+$ to the perturber states $e^3\Sigma^-$ $v = 1$ and 2; $d^3\Delta$ $v = 4$, 5, 6; $a'^3\Sigma^+$ $v = 9$ and 10; $I^1\Sigma^-$ $v = 1$ and 3 obtained from Refs. [10,13,15,16]. Each datapoint from the literature was weighted according to the claimed accuracy. Relative weights of 1.0, 0.2, 0.04,

Table 6. Effective Hamiltonian and matrix elements for a perturbation analysis of the rotational level structure of the $A^1\Pi$ state ($i = 0, 1$) and its perturbing states. For the $A^1\Pi$ diagonal element, the $+$ and $-$ signs refer to the *e*- and *f*-symmetry states, respectively.

	$A^1\Pi(v=i)$	$D^1\Delta(v=0,1,2)$	$I^1\Sigma^-(v=1,2,3)$	$e^3\Sigma^-(v=1,2,3)$	$a'^3\Sigma^+(v=9,10,11)$	$d^3\Delta(v=4,5,6)$
$A^1\Pi$	$T_v+(B\pm\frac{q}{2})\widehat{N}^2$ $-D\widehat{N}^4+H\widehat{N}^6$	$\xi_i(\mathrm{D}_v)\times$ $(\widehat{N}_+\widehat{L}_-+\widehat{N}_-\widehat{L}_+)$	$\xi_i(\mathrm{I}_v)\times$ $(\widehat{N}_+\widehat{L}_-+\widehat{N}_-\widehat{L}_+)$	$\eta_i(\mathrm{e}_v)\widehat{L}\cdot\widehat{S}$	$\eta_i(\mathrm{a}'_v)\widehat{L}\cdot\widehat{S}$	$\eta_i(\mathrm{d}_v)\widehat{L}\cdot\widehat{S}$
$D^1\Delta$		$T_v+B\widehat{N}^2$ $-D\widehat{N}^4+H\widehat{N}^6$	0	0	0	0
$I^1\Sigma^-$			$T_v+B\widehat{N}^2$ $-D\widehat{N}^4+H\widehat{N}^6$	0	0	0
$e^3\Sigma^-$				$T_v+B\widehat{N}^2$ $-D\widehat{N}^4+H\widehat{N}^6$ $+\frac{2}{3}\lambda(3\widehat{S}_z^2\text{-}\widehat{S}^2)$	0	0
$a'^3\Sigma^+$					$T_v+B\widehat{N}^2$ $-D\widehat{N}^4+H\widehat{N}^6$ $+\frac{2}{3}\lambda(3\widehat{S}_z^2\text{-}\widehat{S}^2)+\gamma(\widehat{N}\cdot\widehat{S})$	0
$d^3\Delta$						$T_v+B\widehat{N}^2$ $-D\widehat{N}^4+H\widehat{N}^6$ $+\frac{2}{3}\lambda(3\widehat{S}_z^2\text{-}\widehat{S}^2)$ $+\gamma(\widehat{N}\cdot\widehat{S})+A\widehat{L}_z\widehat{S}_z$ $+\frac{1}{2}A_D\lambda(\widehat{N}^2\widehat{L}_z\widehat{S}_z+\widehat{L}_z\widehat{S}_z\widehat{N}^2)$

0.04 and 0.01 are assigned to the present laser spectroscopy data, the present FTS data, the data from Le Floch [13,15], the data from Morton and Noreau [16], and the data from Herzberg *et al.* [10], respectively. The parameters were initialised using the centrifugal distortion constants D and H, as well as the overall Λ-doubling constant q values of Ref. [13] for $A^1\Pi$ $v = 0$, and using the D constant for $A^1\Pi$ $v = 1$ from Ref. [8]. The Λ-doublet splitting is highly influenced by the local perturbations as has been pointed out in Ref. [13]. We note that the q-parameter could have been set to zero while still retaining the capacity of the model to reproduce the experimental values to a similar accuracy. Presumably this is because the parameters associated with the perturbation already encode the information of Λ-doubling itself. (We note that some hint of a systematic trend in the fitting residues could be observed at high-J levels, however, these are within the measurement uncertainty.) Nevertheless, we retained the q-parameter in the model where the initial parameter values were set to the value in Ref. [13].

The residuals of the combined fit, including literature data and all possible perturbing states, are plotted in Figure 7. The contribution to the rms residual value of laser spectroscopy data is 0.002 cm^{-1} and the contribution of FTS data is 0.014 cm^{-1}. The rms residual value of the combined data set including the less accurate literature data yields 0.09 cm^{-1}, demonstrating that the fitting model satisfactorily reproduces the comprehensive experimental data set. In total, some 787 transitions were used in the global fitting procedure, of which 141 transitions are from the present spectroscopic measurements. Inspection of the correlation matrix indicates a satisfactorily low correlation between the 39 fitted model parameters. We note that judiciously fixing parameters which pertain to molecular constants of perturber states with minimal effect further reduces the correlations between the fitted parameters.

The final set of fitted parameters are summarised in Table 7. For the $A^1\Pi$ $v = 0$ state, the perturbers with significant effect include the $e^3\Sigma^-$ $v = 1$, 2 and 3, $d^3\Delta$ $v = 4$ and 5, $I^1\Sigma^-$ $v = 1$ and 2, $D^1\Delta$ $v = 0$ and 1 and $a'^3\Sigma^+$ $v = 9$ states. For the $A^1\Pi$ $v = 1$ state the perturbers are the $D^1\Delta$ $v = 1$, the $e^3\Sigma^-$ $v = 3$, the $d^3\Delta$ $v = 5$ and 6, $I^1\Sigma^-$ $v = 2$ and 3 and the $a'^3\Sigma^+$ $v = 10$ and 11 states. We note that the molecular constants with an uncertainty indicated within parenthesis () are fitted parameters. The other constants without indicated uncertainty value are taken from literature and fixed during the fitting. It was necessary to fix these parameters to reduce the correlation between parameters.

The improvements in this study mostly affect the molecular constants T_v and B for the $A^1\Pi$ $v = 0$ and 1 and $e^3\Sigma^-$ $v = 1$ states, and for the T_v, B and A constants for the $d^3\Delta$ $v = 5$ state, owing to the more accurate dataset for the low-J transitions in this study. We note that our molecular constants, e.g. T_v and B, are defined differently in Field [8] and Le Floch *et al.* [13] as listed in table 4.2 of Ref. [38]. The definition that we adopt in this study is

Table 7. Compilation of the molecular constants for the $A^1\Pi$ $v = 0$ and $v = 1$ states of $^{12}C^{16}O$ and all perturbing states following from the present analysis. In cases where an uncertainty is specified in () brackets the value was determined from the fit; in cases where this is not specified a value was taken from literature. All values in vacuum cm^{-1}.

Singlet states	$A^1\Pi(v = 0)$	$A^1\Pi(v = 1)$	
T_v	64746.762 (4)	66228.801 (3)	
B	1.604069 (8)	1.58126 (1)	
$q\ (\times\ 10^5)$	3.1 (6)	−2.6 (5)	
$D\ (\times\ 10^6)$	7.348 (8)	7.41 (1)	
$H\ (\times\ 10^{12})$	−9 (2)	−22 (2)	
Triplet states	$e^3\Sigma^-(v = 1)$	$e^3\Sigma^-(v = 2)$	$e^3\Sigma^-(v = 3)$
T_v	64801.136 (4)	65877.55[a]	66934.08[a]
B	1.25708 (3)	1.23909 (2)	1.22273[a]
λ	0.517[a]	0.568[a]	0.778[a]
$D\ (\times\ 10^6)$	6.77[a]	6.75[a]	6.72[a]
$H\ (\times\ 10^{12})$	−2[a]	−2[a]	−2[a]
η_0	15.104 (2)	−17.47 (9)	21.6 (5)
η_1			3.0 (2)
Triplet states	$d^3\Delta(v = 4)$	$d^3\Delta(v = 5)$	$d^3\Delta(v = 6)$
T_v	65102.12 (1)	66173.07 (1)	67225.80[b]
B	1.23327 (1)	1.21628 (4)	1.19941 (3)
A	−16.465 (6)	−16.674 (6)	−16.909[b]
λ	0.993[a]	1.2[a]	1.2[b]
$\gamma\ (\times\ 10^3)$	−8.54[a]	−8[a]	−8[b]
$D\ (\times\ 10^6)$	6.47[a]	6.47[a]	6.44[b]
$H\ (\times\ 10^{12})$	−0.8[a]	−0.8[a]	−0.8[c]
$A_D\ (\times\ 10^4)$	−1[a]	−1[a]	−1[c]
η_0	−21.69 (2)	17.8 (2)	
η_1		−16.916 (5)	18.6 (1)
Triplet states	$a'^3\Sigma^+(v = 9)$	$a'^3\Sigma^+(v = 10)$	$a'^3\Sigma^+(v = 11)$
T_v	65492.66[a]	66520.44[b]	67529.59[b]
B	1.181342[a]	1.16640 (9)	1.14921[b]
λ	−1.153[a]	−1.146[b]	−1.153[b]
$\gamma\ (\times\ 10^3)$	0.72[a]	−0.72[b]	4.47[b]
$D\ (\times\ 10^6)$	6.27[a]	6.26[b]	6.26[b]
$H\ (\times\ 10^{12})$	−0.4[a]	−0.4[d]	−0.4[d]
η_0	2.421[a]		
η_1		4.9 (1)	3.6 (3)
Singlet states	$D^1\Delta(v = 0)$	$D^1\Delta(v = 1)$	
T_v	65421.95[a]	66464.59[a]	
B	1.251[a]	1.233[a]	
$D\ (\times\ 10^6)$	7[a]	7[a]	
$H\ (\times\ 10^{12})$	−0.3[a]	−0.3[a]	
ξ_0	0.030[a]	0.040[a]	
ξ_1		0.073 (4)	
Singlet states	$I^1\Sigma^-(v = 1)$	$I^1\Sigma^-(v = 2)$	$I^1\Sigma^-(v = 3)$
T_v	65617.26[a]	66667.13[a]	67696.60[e]
B	1.24332 (4)	1.2254 (1)	1.20759 (4)
$D\ (\times\ 10^6)$	6.87[a]	6.89[a]	6.89[f]
$H\ (\times\ 10^{12})$	3[a]	3[a]	3[f]
ξ_0	−0.076 (1)	0.085 (3)	
ξ_1		0.079 (2)	0.043 (2)

[a] Data from Ref. [13] and converted, see text. [b] Data from Ref. [38] and converted, see text. [c] Constant fixed to that of $d^3\Delta$, $v = 5$ as first-order approximation. [d] Constant fixed to that of $a'^3\Sigma^+$, $v = 9$ as first-order approximation. [e] Data from Ref. [36]. [f] Constant fixed to that of $I^1\Sigma^-$, $v = 2$ as first-order approximation.

convenient in terms of extracting parameters directly from the fit of the experimental data. In this study the level energy is expressed as a polynomial series in $x = J(J + 1)$, and thus combine effects from molecular parameters of other interacting states. Although an explicit relation between the different definitions can be derived from the effective elements of the Hamiltonian in Ref. [38], not all values of isolated molecular parameters were available, and thus a direct comparison was not possible. In addition, the spin-orbit interaction parameters (η_i) in our definition are larger by a factor $\sqrt{3}$ than in Ref. [8,13]. We note that when the values of parameters are taken from literature (both for fixed parameters and for initialisation of fitted parameters), we have carried out the appropriate conversion by taking into account the definitions of Ref. [38]. The improved constants for $e^3\Sigma^-$ and $d^3\Delta$ in the present analysis stem from the few transitions recorded at much improved absolute accuracy in the present measurements. For the perturber states that affect the low-J rotational states the $A^1\Pi$ $v = 0$ and 1 levels, accurate interaction parameters are obtained from the present deperturbation analysis. The current set of molecular constants gives an accurate description of the structure of $A^1\Pi - X^1\Sigma^+$ (0,0) and (1,0) bands, that improves upon previous analyses. The values of matrix elements for other perturbations occurring at higher J-values are determined but should be treated with some caution. Their purpose is to describe the structure of $A^1\Pi$, $v = 0$ and 1 at the highest level of accuracy; they do not represent physical information at the highest accuracy levels on the perturbation crossings at higher J-values, which were not observed in the present spectroscopic study.

Simulated spectra using the parameters in Table 7 are shown with the FTS spectra in Figure 8 for the $A^1\Pi - X^1\Sigma^+$ (0,0) band and in Figure 9 for the $A^1\Pi - X^1\Sigma^+$ (1,0) band. The positions of the observed transitions belonging to the perturbing $e^3\Sigma^-$ $v = 1$ level and $d^3\Delta$ $v = 5$ level are also indicated in the figures. It should be noted that in addition to $A^1\Pi - X^1\Sigma^+$ transitions, the $d^3\Delta - X^1\Sigma^+$ $v = 5$ transitions have been recently observed in quasar absorption spectra [39].

5. Conclusion

We have obtained high-resolution spectra of the two lowest-v' (0,0) and (1,0) bands of the $A^1\Pi - X^1\Sigma^+$ system of $^{12}C^{16}O$, using two different advanced spectroscopic methods achieving high accuracy on absolute transition frequencies. The combined data were used to perform an improved analysis of the perturbations by a large number of states, in particular of the $e^3\Sigma^- - X^1\Sigma^+$ (1,0) and $d^3\Delta - X^1\Sigma^+$ (5,0) bands, crossing at low values of J. The present analysis is of importance to astronomical observations, where CO is often observed in cold environments with population of $J < 20$ quantum states.

Acknowledgements

This work was supported by the Netherlands Astrochemistry Program of NWO (CW-EW). Staff of the SOLEIL synchrotron is thanked for their hospitality and support.

References

[1] H. Deslandres, Comptes Rendus Acad. Sci. (Paris) **106**, 842 (1888).

[2] J.D. Simmons, A.M. Bass, and S.G. Tilford, Astroph. J. **155** (1), 345 (1969).

[3] R.T. Birge, Phys. Rev. **28**, 1157 (1926).

[4] R. Kepa and M. Rytel, Acta Phys. Polon. A **37**, 585 (1970).

[5] A.C. Le Floch and C. Amiot, Chem. Phys. **97** (1), 379 (1985).

[6] G. Herzberg, Zeitschr. Physik **52**, 815 (1929).

[7] R. Kepa, M. Knotwisniewska, and M. Rytel, Acta Phys. Polon. A **48** (6), 819 (1975).

[8] R.W. Field, B.G. Wicke, J.D. Simmons, and S.G. Tilford, J. Mol. Spectr. **44** (2), 383 (1972).

[9] G. Herzberg and T.J. Hugo, Can. J. Phys. **33**, 757 (1955).

[10] G. Herzberg, T.J. Hugo, S.G. Tilford, and J.D. Simmons, Can. J. Phys. **48** (24), 3004 (1970).

[11] J.D. Simmons and S.G. Tilford, J. Chem. Phys. **45**, 2965 (1966).

[12] G. Herzberg, J.D. Simmons, A.M. Bass, and S.G. Tilford, Can. J. Phys. **44** (12), 3039 (1966).

[13] A.C. Le Floch, F. Launay, J. Rostas, R.W. Field, C.M. Brown, and K. Yoshino, J. Mol. Spectr. **121** (2), 337 (1987).

[14] A.C. Le Floch, J. Rostas, and J. Schamps, Mol. Phys. **63** (4), 677 (1988).

[15] A.C. Le Floch, Ph. D. thesis, Univ. Paris-Sud, 1989.

[16] D.C. Morton and L. Noreau, Astroph. J. Suppl. Ser. **95** (1), 301 (1994).

[17] M. Drabbels, J.J. ter Meulen, and W.L. Meerts, Chem. Phys. Lett. **267** (1–2), 127 (1997).

[18] W. Ubachs, R. Buning, K.S.E. Eikema, and E. Reinhold, J. Mol. Spectr. **241** (2), 155 (2007).

[19] E.J. Salumbides, M.L. Niu, J. Bagdonaite, N. de Oliveira, D. Joyeux, L. Nahon, and W. Ubachs, Phys. Rev. A **86**, 022510 (2012).

[20] G. Guelachvili, D. de Villeneuve, R. Farrenq, W. Urban, and J. Vergès, J. Mol. Spectr. **98** (1), 64 (1983).

[21] T.D. Varberg and K.M. Evenson, Astroph. J. **385** (2), 763 (1992).

[22] N. de Oliveira, D. Joyeux, D. Phalippou, J.C. Rodier, F. Polack, M. Vervloet, and L. Nahon, Rev. Scient. Instr. **80** (4), 043101 (2009).

[23] N. de Oliveira, M. Roudjane, D. Joyeux, D. Phalippou, J.C. Rodier, and L. Nahon, Nat. Photon. **5** (3), 149 (2011).

[24] E.B. Saloman, J. Phys. Chem. Ref. Data **33** (3), 765 (2004).

[25] C.J. Humphreys and E. Paul, J. Opt. Soc. Am. **60** (10), 1302 (1970).

[26] F. Brandi, I. Velchev, W. Hogervorst, and W. Ubachs, Phys. Rev. A **64** (3), 032505 (2001).

[27] W. Ubachs, K.S.E. Eikema, W. Hogervorst, and P.C. Cacciani, J. Opt. Soc. Am. B **14** (10), 2469 (1997).

[28] S. Xu, R. van Dierendonck, W. Hogervorst, and W. Ubachs, J. Mol. Spectr. **201**, 256 (2000).

[29] B. Bodermann, H. Knöckel, and E. Tiemann, Eur. J. Phys. D **19**, 31 (2002).

[30] S. Hannemann, E.J. Salumbides, and W. Ubachs, Opt. Lett. **32** (11), 1381 (2007).

[31] K.S.E. Eikema, W. Ubachs, W. Vassen, and W. Hogervorst, Phys. Rev. A **55** (3), 1866 (1997).

[32] K.D. Bonin and T.J. Mcllrath, J. Opt. Soc. Am. B **1**, 52 (1984).

[33] A.C. Le Floch (private communication 2000).

[34] M. Drabbels, W.L. Meerts, and J.J. ter Meulen, J. Chem. Phys. **99** (4), 2352 (1993).

[35] B.A. Garetz, C. Kittrell, and A.C.L. Floch, J. Chem. Phys. **94**, 843 (1991).

[36] J. Simmons and S. Tilford, J. Res. NBS A. Phys. Ch. **75A** (5), 455 (1971).

[37] C.M. Western, *Pgopher, a Program for Simulating Rotational Structure* (University of Bristol), <http://pgopher.chm.bris.ac.uk>.

[38] R.W. Field, Ph. D. thesis, Harvard University, 1971.

[39] P. Noterdaeme, P. Petitjean, C. Ledoux, S. López, R. Srianand, and S.D. Vergani, Astron. Astrophys. **523**, A80 (2010).